PHOTONICS Research

Fast extended depth of focus meta-optics for varifocal functionality

James E. M. Whitehead,[1] Alan Zhan,[2] Shane Colburn,[2] Luocheng Huang,[1] and Arka Majumdar[1,3,*]

[1]Department of Electrical and Computer Engineering, University of Washington, Seattle, Washington, D.C. 98195, USA
[2]Tunoptix, Seattle, Washington, D.C. 98195, USA
[3]Department of Physics, University of Washington, Seattle, Washington, D.C. 98195, USA
*Corresponding author: arka@uw.edu

Received 25 June 2021; revised 12 January 2022; accepted 1 February 2022; posted 2 February 2022 (Doc. ID 434681); published 1 March 2022

Extended depth of focus (EDOF) optics can enable lower complexity optical imaging systems when compared to active focusing solutions. With existing EDOF optics, however, it is difficult to achieve high resolution and high collection efficiency simultaneously. The subwavelength spacing of scatterers in a meta-optic enables the engineering of very steep phase gradients; thus, meta-optics can achieve both a large physical aperture and a high numerical aperture. Here, we demonstrate a fast ($f/1.75$) EDOF meta-optic operating at visible wavelengths, with an aperture of 2 mm and focal range from 3.5 mm to 14.5 mm (286 diopters to 69 diopters), which is a 250× elongation of the depth of focus relative to a standard lens. Depth-independent performance is shown by imaging at a range of finite conjugates, with a minimum spatial resolution of ∼9.84 μm (50.8 cycles/mm). We also demonstrate operation of a directly integrated EDOF meta-optic camera module to evaluate imaging at multiple object distances, a functionality which would otherwise require a varifocal lens.

https://doi.org/10.1364/PRJ.434681

1. INTRODUCTION

Optical imaging systems operating at finite conjugates suffer from a limited depth of focus. This often necessitates complex refocusing mechanisms. While large scale optics can be refocused by manually translating individual elements, integrated applications require high-precision actuators and active feedback to modify the optics. Several active solutions are currently used to adjust the focal plane in integrated systems such as electro-wetting [1–3], stretchable membranes, and MEMS actuation [4–6]. These solutions, however, have various drawbacks such as delicate control mechanisms, extra electrical circuitry, multiple acquisitions, and temperature sensitivity. Additionally, most of the electro-mechanically tunable optics are limited to small apertures (<500 μm), not conducive for many practical applications. Instead of dynamically changing the focal plane, a static optic with an extended focal zone can be used to image all objects in a desired depth covered by the focal range [7]. For conventional lenses, the depth of focus is inversely proportional to the square of the numerical aperture (NA $\sim \frac{D}{2f}$), where D is the diameter and f is the focal length of the lens. This leads to a trade-off between the depth of focus and resolution. The depth of focus of any lens can be increased by reducing the NA, but that limits the achievable resolution of the optical system due to the diffraction limit. Additionally, for many practical applications, we need a sufficiently large diameter lens to ensure collection of enough photons to achieve an acceptable signal-to-noise ratio.

Extended depth of focus (EDOF) refractive lenses have been demonstrated in the past by exploiting wavefront coding [7–9]. Typically, a phase-plate is added in front of a refractive lens to obtain the EDOF property. With the need for miniaturizing imaging systems for emerging applications like autonomous navigation, smart home, and the Internet of Things, there is a growing trend of migrating from refractive elements to flat diffractive optics. Unsurprisingly, EDOF concepts have also been demonstrated in diffractive optics in the recent past. Specifically, exploiting inverse design, an extreme depth of field for an EDOF lens was reported using multi-level diffractive optics [10]. The reported 1.8 mm EDOF lens had a smallest focal length of 5 mm, with the maximum NA being 0.16.

Meta-optics are subwavelength diffractive optics, which can guide all the light to the zeroth order and can provide a full 2π phase shift using a binary photo-mask [11,12], making them compatible with a single stage lithography process. Owing to their subwavelength pitch, meta-optics can support higher phase gradients and, thus, larger NA compared to multi-level diffractive optics. EDOF meta-optics have previously been utilized to mitigate chromatic aberrations in full-color imaging [13,14]. Recently, inverse design techniques have also been used to create EDOF meta-optics [15,16]; however, the utility

of EDOF meta-optics for finite conjugate imaging at different object and image distances has not been demonstrated. In this work, we report a 2 mm diameter EDOF meta-optic with a maximum NA of 0.28 (f-number: 1.75). This is the highest NA EDOF optic for varifocal imaging reported to date. The EDOF is 11 mm (from 3.5 mm to 14.5 mm); thus, the optical power in this system can be changed from 69 diopters to 286 diopters. We note that, for a standard hyperboloid lens with a focal length at the center of the above range, the depth focus is expected to be only $\sim 4\lambda(\frac{f}{D})^2 \approx 43$ μm for green light. Thus, our EDOF meta-optic shows a 250× elongation of the depth of focus compared to a standard lens. We also demonstrate imaging in multiple finite conjugate planes, where the required focal length changes from 3.65 mm to 7.55 mm, and we achieved a resolution of ~9.84 μm (50.8 cycles/mm) in the object plane. Finally, we report direct integration of the meta-optic into a commercial camera module and show imaging at different object planes. We emphasize that this is the first time a visible EDOF meta-optic is directly integrated on a sensor, and no other relay optics were employed for imaging. Thus, exploiting a static meta-optic and computational back end, we can implement some functionalities of a varifocal lens. Transferring such optical functionality into the software could foster a new era of "software-defined optics."

2. DEVICE DESIGN AND FABRICATION

There are several different types of EDOF meta-optics that have been reported in the literature before [14]. In this work, we employ a cubic EDOF [13] with the following phase profile:

$$\phi(x,y) = \frac{2\pi}{\lambda}\left(\sqrt{x^2+y^2+f^2} - f\right) + \frac{\alpha}{R^3}(x^3+y^3).$$

Here, λ is the operating wavelength, x and y are the cartesian coordinates, f is the nominal focal length of the lens, R is the radius of the phase mask, and α determines the strength of the cubic component. With increasing α, we can extend the depth of focus more, at the cost of decreasing signal to noise ratio [17]. For our meta-optic, we set α to be 100π, $R = 1$ mm, and $f = 5.6$ mm. These parameters are chosen by performing numerical simulations to ensure high NA and large depth of focus. The aperture of the lens is chosen under the constraints of fabrication feasibility. The choice of the cubic phase profile is primarily motivated by its closed form expression and interpretability of the equation. The closed form expression allows us to design the meta-optics at arbitrary apertures and focal lengths, unlike inverse-designed techniques, which will require redesigning the meta-optics with many changed parameters. Moreover, with larger apertures, the inverse design techniques require a large amount of computational resources. While the cubic phase profile makes the design simple, we cannot ensure this is the most optimal solution for EDOF, for which inverse design can be employed. However, Dowski *et al.* derived the cubic phase profile as an optical form that is invariant to defocus based on mathematical analysis of the optical misfocus function [7]. We note that a similar cubic EDOF meta-optic has been used before [13] for full-color imaging, but no varifocal functionality was demonstrated. Additionally, the previous meta-optics only had a 200 μm aperture, and the imaging was performed using a relay microscope optic.

We used silicon nitride (SiN) pillars on silica as the scatterers for the meta-optic [Fig. 1(a)]. For the scatterers, we used square posts to ensure polarization-insensitive operation and large phase coverage for a given height, as well as faster writing speeds using the electron-beam lithography tool. We simulate the transmission characteristics of these square posts using Lumerical FDTD Solutions under a periodic boundary condition to ensure we have high transmission while covering the whole 0–2π phase shift [Fig. 1(b)]. The meta-optic is then created by mapping the desired phase to the appropriate scatterer geometry under the local phase approximation [12,18]. A cubic meta-optic does not produce a point-like point spread function (PSF), and to extract the depth of focus, we calculate the correlation of the PSF along the optical axis [14] [Fig. 1(e)] using $\mathrm{Corr}(x,y) = \sum_i \frac{(x_i-\bar{x})(y_i-\bar{y})}{\sqrt{\sum(x_i-\bar{x})^2 \sum(y_i-\bar{y})^2}}$, where, x_i and y_i are the

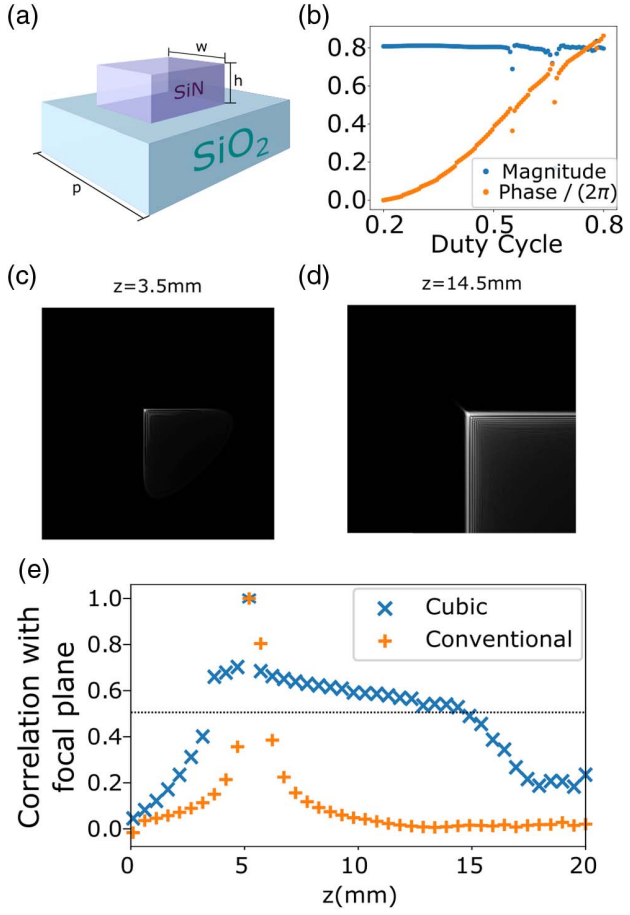

Fig. 1. Scatterer and meta-optics design and simulation. (a) Schematic of $h = 633$ nm thick SiN square posts on a silicon oxide substrate. The periodicity p is kept constant, and the width w is changed to cover the whole 0–2π phase. (b) Magnitude and phase of the transmitted light for a plane wave input with $p = 350$ nm. (c) and (d) are simulated PSFs of the EDOF meta-optic at object distances of 3.5 mm and 14.5 mm, respectively. (e) Correlation plot of simulated PSF against the PSF at the central focal point for a cubic meta-optic and a conventional metalens. The correlation clearly shows the extension of the depth of focus.

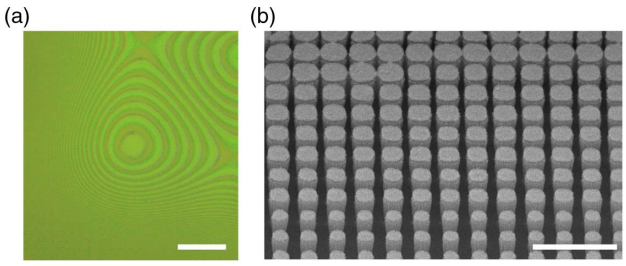

Fig. 2. Images of the fabricated meta-optics. The meta-optic was sputter coated with gold-palladium alloy to ensure charge dissipation during imaging. (a) Optical image (scale bar is 150 μm) shows that the fabricated meta-optic is not centrosymmetric. (b) Scanning electron micrograph; scale bar of 1 μm taken at 45° to the normal.

individual elements of the 2D PSF and $\bar{x}$ and $\bar{y}$ are the averages of the 2D PSFs. Here we use the PSF at the nominal focal length as the reference, making the correlation value unity at the nominal focal length. We define the depth of focus as the range where the correlation value stays above 0.5. From the numerical analysis, we estimate the depth of focus to be 11 mm, with a minimum focal length of 3.5 mm. This makes the maximum NA of the lens 0.28. Figures 1(c) and 1(d) show the simulated PSF of the cubic EDOF at the minimum and maximum focal distances.

Figure 2 shows the optical and scanning electron microscopy (SEM) images of the fabricated EDOF meta-optic (the details of the fabrication can be found in Appendix A).

3. MEASUREMENT

The meta-optic was mounted in a 1 cm diameter optic holder with standard C-mount threading for characterization. The PSF of the meta-optic was measured: a 25 μm diameter pinhole was used to approximate a point source, which was illuminated using a green (Thorlabs M530F1) light emitting diode (LED) with an optical bandwidth of ∼30 nm. The PSF was captured using a movable microscope [Fig. 3(a)]. The position of the pinhole was changed from 7.3 mm to 15.1 mm away from the meta-optic, and the same range is used for the position of the camera [Fig. 3(b)]. It was clearly observed that the PSF remained relatively unchanged for various image and object distances, especially compared to a hyperboloid lens. We note that we measured the PSF for a finite conjugate system, as we used a similar setup for imaging as well. We also confirmed that the minimum focal length for our meta-optic is ∼3.5 mm, making the highest NA of the meta-optic 0.28, as predicted by the numerical simulation. This higher NA compared to previously reported diffractive EDOF lens [10] is due to the subwavelength periodicity and, hence, the ability to sample the phases with finer spatial resolution.

We then tested our system by imaging a 1951 USAF resolution chart. The images of this backlit pattern were taken at various object (u) and image (v) distances to test the EDOF capability of the lens. From ray optics, we can write for a lens with focal length f,

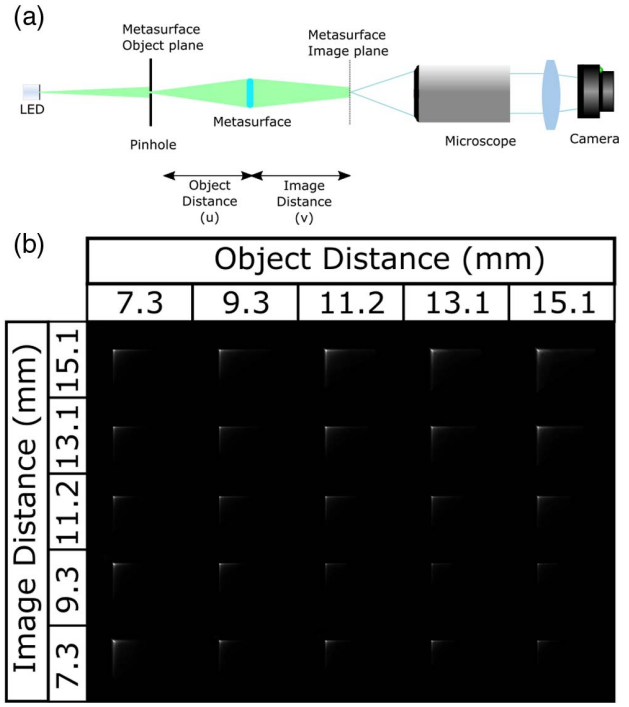

Fig. 3. (a) Setup for PSF measurement. (b) Image of 25 μm pinhole. Image and object plane sweep. Illumination is using a 530 nm LED with 33 nm bandwidth.

$$\frac{1}{u}+\frac{1}{v}=\frac{1}{f}.$$

As a cubic EDOF meta-optic does not produce a lens-like PSF and the raw captured images do not resemble the object, the captured sensor data must be deconvolved to extract the in-focus image. Several different deconvolution routines, including Wiener, Richardson–Lucy, and learned methods, can be used to extract the image [19,20]. Here, we apply a routine based on total variation (TV) regularization to deconvolve and denoise the latent image [Fig. 4(a)]. This deconvolution method optimizes the sum of the gradient magnitudes while deconvolving the image [21]. As we are imaging under incoherent illumination, we can approximate the whole imaging process as a linear system if the camera is not saturated. We ensured that the intensity of the measured PSF did not exceed the maximum threshold of the camera to conserve the linearity of the measured PSF. We also assumed that the PSF was shift-invariant. This assumption breaks down for large lateral displacements of the pinhole, and taking multiple shifted PSFs while using a shift-variant deconvolution technique may produce better results [19]. In our work, this means we have a constrained field of view to ensure the shift-invariant property of our PSF. The imaging here shows the same range of tunable focal lengths as from the PSF measurements. We estimate the spatial resolution of our meta-optic via the linecuts from the measured patterns for an object (image) distance of 9.3 mm (13.1 mm) [Fig. 4(b)]. The first column shows the linecuts from the horizontal lines, and the vertical lines are shown in the second column. We can see that, for the horizontal lines, we can differentiate lines of thickness of ∼9.84 μm

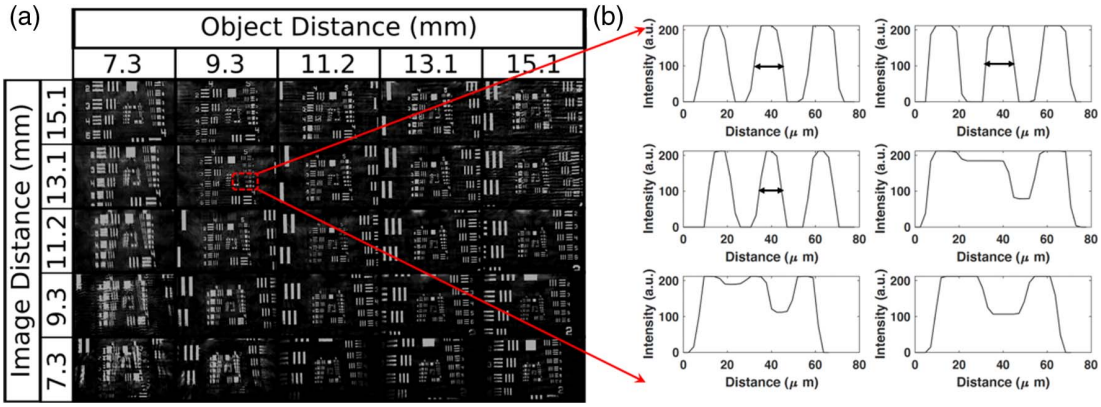

Fig. 4. (a) Image of the airforce resolution chart for different image and object planes. The object distance is the separation between the transparency and the meta-optic while the image distance is the distance between the meta-optic and the camera. The object is illuminated via a 530 nm LED with 33 nm bandwidth (full width at half-maximum). (b) Linecut of the air force chart (for object distance of 9.3 mm and image distance of 13.1 mm) to estimate resolution: first column is for horizontal lines, and second column is for vertical lines. Top to bottom rows, group 5, number 4–6 for the airforce resolution chart.

(50.8 cycles/mm), whereas, for vertical lines, only ∼11.05 μm lines (45.3 cycles/mm) can be resolved. We attribute this asymmetry to the asymmetric PSF of the cubic EDOF meta-optics. The diffraction limited resolution for a lens under the same condition is ∼1.4 μm. The lower spatial resolution comes from the extended PSF of the cubic meta-optic compared to a lens. As explained earlier, however, the EDOF meta-optic can be used to create images for different object and image distances, which is not possible with an ordinary metalens.

Thus far in our experiments, we have used a microscope to relay the image produced by the EDOF meta-optic onto the sensor for imaging. With a larger aperture meta-optic, it is feasible to image directly onto an off-the-shelf camera module (E-con Systems See3CAM_10CUG). For integration, the meta-optic was mounted in a C-thread optic mount (Edmund Optics #63-979). The meta-optic was then attached to the camera module using a CS-mount, with a flange back distance of approximately 12 mm. The final package is shown in Fig. 5(a). In this configuration, the imaging system has a full diagonal field of view of 28°. We note that there are very few demonstrations of direct integration of visible meta-optics on sensors [22], primarily because many of the visible meta-optics have very small aperture (∼50–200 μm). As most commercial sensors have a thick glass plate on top of the bare sensor, an aperture that is greater than 1 mm is required to have a reasonable NA.

We tested the imaging capabilities of the EDOF camera and compared it to an off-the-shelf plano–convex *F*/2 refractive singlet with focal length 6 mm (Edmund Optics #32-952) by imaging a series of QR codes at different object distances. Both the EDOF meta-optic and refractive singlet lens are tested using the same camera module and with the same CS-mount, ensuring the same sensor characteristics and magnification. The QR codes are illuminated using a commercially available green LED ring light. The EDOF meta-optic and the refractive singlet have nominal focal lengths that are optimal for imaging at a finite conjugate distance of 13 mm. As seen in the Fig. 5(b), both imaging systems are fully capable of resolving the QR

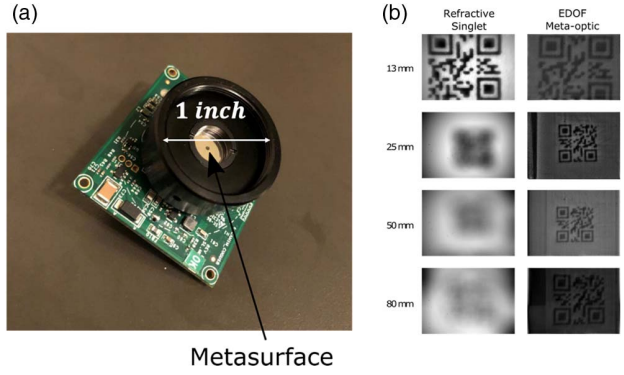

Fig. 5. (a) Metasurface optic integrated with E-con Systems camera module. (b) Pictures of QR code object at differing object lengths taken by a singlet refractive lens with focal length 6 mm at *F*/2 (left) and by a singlet EDOF meta-optic with nominal focal length 5.6 mm at *F*/2.8 (right). The 13 mm and 25 mm object distances used a 5 mm × 5 mm QR code. The 50 mm object distance used a 10 mm × 10 mm QR code, and the 80 mm object distance used a 30 mm × 30 mm barcode.

code, but the refractive singlet displays improved brightness and contrast when compared to the EDOF meta-optic. As we move the object plane further out, however, the difference between the EDOF meta-optic and refractive singlet widens. For object distances of 25 mm, 50 mm, and 80 mm, the refractive singlet is incapable of resolving the QR code, while the EDOF meta-optic reliably resolves the barcodes throughout the range of object distances. We note that this range is chosen arbitrarily to demonstrate the varifocal functionality of our EDOF meta-optics. The range can be increased by increasing the value of the parameter α, albeit at the cost of lower SNR.

When compared to our EDOF meta-optic (*F*/2.8, focal length 5.6 mm), the refractive singlet has a similar focal length (6 mm versus 5.6 mm) but a larger diameter (3 mm versus 2 mm). The superior brightness and contrast of the singlet

at the object distance of 13 mm are attributed both to the larger diameter of the refractive singlet and also the properties of the EDOF meta-optic itself. At an aperture of 3 mm, the refractive optic has a surface that has twice the area of the EDOF meta-optic and is able to more than double the light collection. In addition, the EDOF meta-optic operates by sacrificing some contrast at the nominal object distance in favor of extending the depth of field significantly.

4. DISCUSSION

We reported an EDOF, $f/1.75$ cubic meta-optic with a highest NA of 0.28, leveraging the subwavelength pitch of meta-optics to enable fast lensing. The EDOF nature of the meta-optic was evaluated using PSF measurements and imaging experiments. We also reported the development of an EDOF meta-optic camera module using a commercial sensor and demonstrated QR code imaging at different object distances. Compared to a traditional lens, we can get in-focus images over a longer depth of focus. The use of a cubic phase profile to obtain the EDOF property comes at the cost of a large PSF, which reduces the SNR of the reconstructed image. Inverse-design techniques can be used to mitigate this reduction in SNR by making EDOF meta-optics with lens-like PSF [16] and optimized Strehl ratio. We also note that, while EDOF meta-optics themselves can be used to perform broadband imaging [13,14], the demonstrated varifocal functionality works only for a narrowband light-source (linewidth of ∼30 nm). However, by engineering the phase profile or using a hybrid refractive-diffractive optic, both broadband and EDOF properties can potentially be realized [23]. Finally, a serious problem in meta-optics is fabrication imperfections. Based on our numerical analysis, with a random variation of pillar diameters by ±5%, we did not find any noticeable change in the parameters of the optics. We note that the EDOF nature of the optics also makes the optics more robust against fabrication disorders, as the slight change in the focal lengths has no effect on the performance.

Our work opens opportunities for system-level integration of meta-optics with commercial sensors, and the simplification of tunable imaging systems exploiting EDOF properties. This new class of EDOF imaging systems could find applications in industrial production lines [24], compact image sensors, biological imaging [25,26], automobile navigation, and driver monitoring systems. Going beyond EDOF, such software-defined optics could potentially transfer many of the hardware functionalities to software and accelerate the co-design and co-integration of hardware and software for free-space optics.

APPENDIX A: FABRICATION METHODS

We used a 1.3 mm thick, 1 cm diameter silica mirror blank from Edmund Optics as a substrate. The choice of this wafer is motivated by its compatibility with commercial optical mounts. The double side polished silica wafer was cleaned in a boiling solution of sulfuric acid and hydrogen peroxide for 10 min. Plasma-enhanced chemical vapor deposition was then used to deposit a 633 nm layer of SiN on one side. A layer of 200 nm ZEP-520A positive tone electron-beam resist was spun after a short clean in oxygen plasma to maximize adhesion. An estimated 8 nm of Au/Pd was sputtered to dissipate charge produced from the electron beam. The pattern was written using electron-beam lithography (JEOL JBX6300FS at 100 kV). The Au/Pd layer was then subsequently removed by immersing in Transene Gold Etchant Type TFA with mild agitation. The resist was developed in Amyl acetate and rinsed in isopropyl alcohol, followed by a Descum process in a weak oxygen plasma. A layer of 50 nm nickel with a 5 nm chromium adhesion layer was then deposited using an electron-beam evaporator. Parts of the deposited Ni/Cr metal were removed by dissolving the supporting resist in a solvent while sonicating. An inductively coupled fluorine plasma etcher (Oxford Plasmalab 100) etched the exposed SiN down to the substrate, and the Ni/Cr metal hard mask was removed with nickel and chromium etchants. The metasurface was then cleaned again with a boiling solution of sulfuric acid and hydrogen peroxide for 10 min. Using direct write photolithography and electron-beam evaporation, a chromium aperture was patterned to block stray light from bypassing the meta-optics.

Funding. DARPA (140D0420C0060); Tunoptix; National Science Foundation (NNCI-2025489, NNCI-1542101).

Acknowledgment. The research is supported by Tunoptix and DARPA. A. M. is also supported by a Washington Research Foundation distinguished investigator award. Part of this work was conducted at the Washington Nanofabrication Facility/Molecular Analysis Facility, a National Nanotechnology Coordinated Infrastructure (NNCI) site at the University of Washington with partial support from the National Science Foundation.

Disclosures. A. M., A. Z., and S. C. are involved with the startup Tunoptix Inc., which is commercializing technology discussed in this paper.

REFERENCES

1. S. W. Seo, S. Han, J. H. Seo, Y. M. Kim, M. S. Kang, N. K. Min, W. B. Choi, and M. Y. Sung, "Microelectromechanical-system-based variable-focus liquid lens for capsule endoscopes," Jpn. J. Appl. Phys. **48**, 052404 (2009).
2. H.-S. Ee and R. Agarwal, "Tunable metasurface and flat optical zoom lens on a stretchable substrate," Nano Lett. **16**, 2818–2823 (2016).
3. S. M. Kamali, E. Arbabi, A. Arbabi, Y. Horie, and A. Faraon, "Highly tunable elastic dielectric metasurface lenses," Laser Photon. Rev. **10**, 1002–1008 (2016).
4. E. Arbabi, A. Arbabi, S. M. Kamali, Y. Horie, M. Faraji-Dana, and A. Faraon, "MEMS-tunable dielectric metasurface lens," Nat. Commun. **9**, 812 (2018).
5. Z. Han, S. Colburn, A. Majumdar, and K. F. Böhringer, "MEMS-actuated metasurface Alvarez lens," Microsyst. Nanoeng. **6**, 79 (2020).
6. Z. Han, S. Colburn, A. Majumdar, and K. F. Bohringer, "Millimeter-scale focal length tuning with MEMS-integrated meta-optics employing high-throughput fabrication," arXiv:2111.07477 (2021).
7. E. R. Dowski and W. T. Cathey, "Extended depth of field through wave-front coding," Appl. Opt. **34**, 1859–1866 (1995).
8. Z. Zalevsky, "Extended depth of focus imaging: a review," SPIE Rev. **1**, 018001 (2010).
9. R. K. Maia, "Extended depth of focus IOLs: the next chapter in refractive technology?" J. Refract. Surg. **33**, 146–149 (2017).

10. S. Banerji, M. Meem, A. Majumder, B. Sensale-Rodriguez, and R. Menon, "Extreme-depth-of-focus imaging with a flat lens," Optica **7**, 214–217 (2020).
11. S. M. Kamali, E. Arbabi, A. Arbabi, and A. Faraon, "A review of dielectric optical metasurfaces for wavefront control," Nanophotonics **7**, 1041–1068 (2018).
12. A. Zhan, S. Colburn, R. Trivedi, T. K. Fryett, C. M. Dodson, and A. Majumdar, "Low-contrast dielectric metasurface optics," ACS Photon. **3**, 209–214 (2016).
13. S. Colburn, A. Zhan, and A. Majumdar, "Metasurface optics for full-color computational imaging," Sci. Adv. **4**, eaar2114 (2018).
14. L. Huang, J. Whitehead, S. Colburn, and A. Majumdar, "Design and analysis of extended depth of focus metalenses for achromatic computational imaging," Photon. Res. **8**, 1613–1623 (2020).
15. E. Bayati, R. Pestourie, S. Colburn, Z. Lin, S. G. Johnson, and A. Majumdar, "Inverse designed metalenses with extended depth of focus," ACS Photon. **7**, 873–878 (2020).
16. E. Bayati, R. Pestourie, S. Colburn, Z. Lin, S. G. Johnson, and A. Majumdar, "Inverse designed extended depth of focus meta-optics for broadband imaging in the visible," Nanophotonics (2021). https://doi.org/10.1515/nanoph-2021-0431.
17. W. T. Cathey and E. R. Dowski, "New paradigm for imaging systems," Appl. Opt. **41**, 6080–6092 (2002).
18. R. Pestourie, C. Pérez-Arancibia, Z. Lin, W. Shin, F. Capasso, and S. G. Johnson, "Inverse design of large-area metasurfaces," Opt. Express **26**, 33732–33747 (2018).
19. E. Tseng, S. Colburn, J. Whitehead, L. Huang, S.-H. Baek, A. Majumdar, and F. Heide, "Neural nano-optics for high-quality thin lens imaging," Nat. Commun. **12**, 6493 (2021).
20. U. Akpinar, E. Sahin, M. Meem, R. Menon, and A. Gotchev, "Learning wavefront coding for extended depth of field imaging," arXiv:1912.13423 (2020).
21. P. Getreuer, "Total variation deconvolution using split Bregman," Image Process. Line **2**, 158–174 (2012).
22. B. Xu, H. Li, S. Gao, X. Hua, C. Yang, C. Chen, F. Yan, S. N. Zhu, and T. Li, "Metalens-integrated compact imaging devices for wide-field microscopy," Adv. Photon. **2**, 026003 (2020).
23. S. R. M. Rostami, S. Pinilla, I. Shevkunov, V. Katkovnik, and K. Egiazarian, "Power-balanced hybrid optics boosted design for achromatic extended depth-of-field imaging via optimized mixed OTF," Appl. Opt. **60**, 9365–9378 (2021).
24. Edmund Optics, "Liquid lenses in machine vision," https://www.edmundoptics.com/ViewDocument/EO_Liquid_Lenses_in_Machine_vision_0419_EN.pdf (2019).
25. B. Forster, D. Van De Ville, J. Berent, D. Sage, and M. Unser, "Complex wavelets for extended depth-of-field: a new method for the fusion of multichannel microscopy images," Microsc. Res. Tech. **65**, 33–42 (2004).
26. F. Aguet, D. Van De Ville, and M. Unser, "Model-based 2.5-D deconvolution for extended depth of field in brightfield microscopy," IEEE Trans. Image Process. **17**, 1144–1153 (2008).